Investigation of the multiphoton excitation process of the $4f^25d$ configuration in $LiYF_4$ and $LiLuF_4$ crystals doped with trivalent neodymium ion

A. F. H. Librantz,[a] L. Gomes, L. V. G. Tarelho, and I. M. Ranieri
Centro de Lasers e Aplicações, IPEN-SP, Travessa R 400, Cidade Universitária, Caixa Postal 11049, CEP 05422-970, São Paulo, Brazil

(Received 4 September 2002; accepted 18 November 2003)

Ultraviolet (UV) fluorescence of Nd^{3+} ions induced by multistep laser excitation was investigated in Nd-doped $LiYF_4$ and $LiLuF_4$ crystals using a technique of time-resolved spectroscopy. The observed UV luminescence was due to transitions between the bottom of $4f^25d$ configuration and the $4f^3$ states of Nd^{3+} ions. The first absorption band of $4f^25d$ configuration, which starts around 56 700 cm^{-1}, was excited by three stepwise absorptions of photons in the green (500–535 nm) from a short pulse laser excitation leading to broad emission bands in UV range (180–280 nm). An excitation band in the blue (468–486 nm) was observed due to the excitation of the second absorption band of $4f^25d$ configuration around 63 000 cm^{-1} according to the photon absorption sequence: $^4I_{9/2}+h\nu(480\,\text{nm})\rightarrow{}^2G(1)_{9/2}+h\nu(480\,\text{nm})\rightarrow{}^2F(2)_{7/2}+h\nu(480\,\text{nm})\rightarrow 4f^25d(\text{second})$. The observed UV emissions (180–280 nm) from the bottom of the $4f^25d$ configuration (first state) have a lifetime of 35 ns (parity allowed) and are broadband in contrast to UV emissions from $4f^3$ configuration, which are also present in the luminescence investigation but having a longer lifetime (8.5 μs) and structures composed of narrow lines. The excitation spectrum of fast UV luminescence exhibited different structures depending on the excitation geometry (σ or π) with respect to the c axis of the crystal. We observed two emissions from the first state of $4f^25d$ configuration with peaks at 535 and 595 nm modifying the luminescence branching ratio of the bottom of the $4f^25d$ configuration around 55 500 cm^{-1}. The equivalent cross section of three and two excitation processes was estimated at 510 nm by solving the rate equations of the system under short laser excitation, which shows that is possible to have laser action under pulsed laser pumping with intensity below the crystal damage threshold. © *2004 American Institute of Physics.*
[DOI: 10.1063/1.1640456]

I. INTRODUCTION

Rare earth (RE^{3+})-doped crystals are widely employed as efficient laser material for generating laser radiation mainly in the infrared region, rarely in the visible, based on the radiative transitions within the $4f^n$ electronic configuration. On the other hand, radiative transitions from the $4f^{n-1}5d$ levels are not very exploited, besides the intrinsic potential to achieve laser action. In spite of this, laser action in the blue, ultraviolet (UV), and vacuum ultraviolet (VUV) spectral range have been demonstrated for Ce^{3+} doped $LiLuF_4$ (LLF)[1] and Nd^{3+} doped $LiYF_4$ (YLF).[2] Recently, the UV and VUV fluorescence of RE^{3+} ions has been extensively investigated because of the growing of applications in this spectral range, such as generating and detecting VUV radiation.[3] This study includes the investigation of UV fluorescence in heavy[4] and light lanthanides.[5] Solid-state fluoride materials doped with Nd^{3+} is a very promising laser medium emitting in the UV region.[6] This system may allow the construction of the first solid-state tunable UV lasers based on the broadband UV emissions of Nd^{3+} at 182, 186, 230, and 262 nm. An other application is the illustration of the photoionization mechanism involving indium ions.[7] The Nd^{3+} excitation can be performed directly to the level of interest with excimer, synchrotron, x-ray radiation sources,[8,9] or sequentially pumped with two-photon[10–12] or three-photon excitation.[13] Despite the direct pumping being more efficient, the lasers applied to excite the UV by a single photon are very expensive and hard to handle, like excimer lasers. The three photon excitation investigated here is based on a high intensity laser pumping in the visible and has the advantage of matching the second harmonic of Nd:YAG laser which is one of the most disseminated lasers for optical pumping systems.[14,15] The $4f^n\leftrightarrow 4f^{n-1}5d$ are parity allowed transitions exhibiting a measured fluorescence lifetime of 35 ns (observed for the case of first and second excitation bands of $4f^25d$ configuration). They are characterized by a stronger environmental interaction and a broadband absorption and emission spectra in the UV range and much higher oscillator strength than the $4f^n$ internal transitions. The $4f^n\rightarrow 4f^n$ transitions are parity forbidden and composed of narrow lines of weak strengths mostly due to the forced electric–dipole interaction induced by odd terms of the local crystal field.[16,17]

The spectrum characterization of the $4f^3\rightarrow 4f^25d$ and $4f^3\rightarrow 4f^3$ transitions of Nd^{3+} provide information about the

[a]Author to whom correspondence should be addressed; electronic mail: lgomes@net.ipen.br

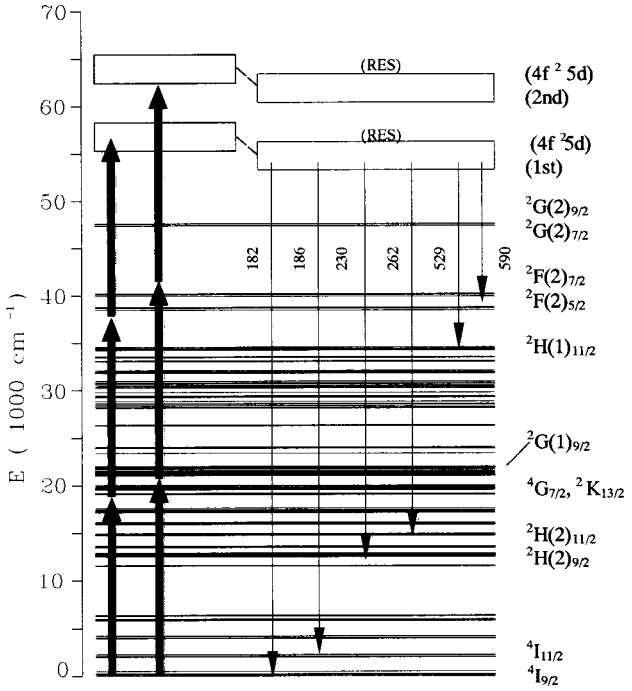

FIG. 1. Schematic diagram of the energy levels of Nd^{3+} ions in YLF showing the multiphoton excitation processes and the fast UV luminescence from the $[^4K_{11/2}]$ state of $4f^25d$ configuration. The level positions, as well as the Stoke's shift were obtained from Refs. 22 and 23.

local level structure and electron–phonon coupling differences between $4f^3$ and the $4f^25d$ electronic configurations because the crystal-field perturbation strength is stronger for electrons in the $5d$ level than for those in the $4f$ level.[18] This results in broadband transition with a large Stokes shift of the emission peak and a high probability for phonon-assisted transitions. We found in the literature that there is an energy difference between the first absorption band of $4f^25d$ configuration centered at 175.4 nm[19,20] and the corresponding emission band from $4f^25d$ to the $^4I_{9/2}$ ground state of Nd^{3+} in YLF with maximum at 181.8 nm.[21] An energy dissipation of $\sim$2000 cm^{-1} is produced by *N*-phonons emission in order to reach the relaxed excited state (RES) of the bottom of the $4f^25d$ configuration at around 55 500 cm^{-1}. This relaxation behavior of the first excited state of $4f^25d$ configuration is expected considering that the electron–phonon coupling increases with the $5d$ orbital overlap ($S_0 \sim 3.5$ considering the cutoff phonon emission of $\hbar\omega \sim 570$ cm^{-1} in YLF). The pumping scheme used in this work is illustrated in Fig. 1. The energy of levels of $4f^3$ states of Nd^{3+} in YLF were obtained from Refs. 22 and 23.

II. EXPERIMENT

Single crystals doped with neodymium were grown by the Czochralski technique under a purified argon atmosphere.[24] The starting growth material was doped with 3 mol % of Nd. The Nd concentration of 1.3 mol % was determined in the samples used in this work by the x-ray fluorescence technique. The YLF and LLF samples were cut and polished properly with the *c* axis parallel to the longest side of the rectangular faced samples. The absorption spectra were carried out using a CARY-OLIS 17D double-beam spectrophotometer interfaced to a computer. A time-resolved spectroscopy system of 10 ns of resolution provided the emission spectra and the decay time determination. The laser pumping system consists of an optical parametric oscillator (OPO), from OPOTEK, pumped by the third harmonic of a Nd:YAG (355 nm) laser (Brilliant B from Quantel) tunable in the visible range from 420 to 680 nm, which delivers a typical energy of 20 mJ with a repetition rate of 10 Hz with a laser pulse duration of 4 ns. The luminescence spectrum in the visible and UV range were analyzed using a 0.25 m monochromator (KRATOS) with an optical grating with blaze at 300 nm. The luminescence was collected perpendicularly to the laser excitation in order to minimize the laser scattered light. A CaF_2 lens was used to collect the luminescence and a refrigerated (-30 °C) photomultiplier with a S-20 type cathode (EMI QB-9558) with a shunt resistance of 50 Ω was used to detect the luminescence signals. The luminescence decay times were recorded using a 100 mega samples per second digital oscilloscope (TDS 410 Tektronix). Luminescence spectrum was spectrally discriminated using a signal processing boxcar averager (PAR 4402) operating with the static gate mode with a sample point of 40 ns (for the fast emission) and 8 μs (for the case of slow component). Both equipments are interfaced to a microcomputer. In all the experiments using the laser to induce the multiphoton excitation, the laser beam was slightly focused in the sample exhibiting a spot of $\sim$0.5 mm^2 to avoid the crystal damage and to minimize the crystal stress that scatters the UV luminescence and therefore decreases the signal to noise ratio.

III. RESULTS AND DISCUSSION

A. Excitation spectra

Using a tunable laser excitations in the visible range generated by the OPO laser pumped by the 355 nm of the Nd:YAG laser with laser pulses of 10 mJ (4 ns and 10 Hz), we could efficiently excite the first and the second excitation bands of $4f^25d$ configuration of Nd^{3+} in both YLF and LLF crystals. The excitation spectrum of the fast UV luminescence (35 ns) was measured by fixing the analyzer monochromator at 262 nm and working with the boxcar averager in static gate mode operation with a sample point of 40 ns (gate width of 2 ns) for the $4f^25d$ excitation spectrum discrimination. The tunable laser excitations produced by the OPO system in the visible range, could excite the Nd^{3+} ion to the $^4G_{7/2}$, $^2F(2)_{5/2}(4f^3)$ and the first and second excited states of $4f^25d$ configuration, respectively, by one, two, and three photon processes. The excitation in the green excites exclusively the first band of $4f^25d$ configuration, while the laser excitation in the blue primarily pumps Nd^{3+} to the second excited state of the $4f^25d$ configuration that in turn populates the lowest one. The excitation process of $4f^25d$ configuration in the blue region constitutes a multiphoton excitation in Nd^{3+} in YLF and LLF crystals. In addition, we did not find the existence of UV and visible luminescence spectrum in pure and undoped crystals under similar laser excitation intensities in the visible range, which indicates

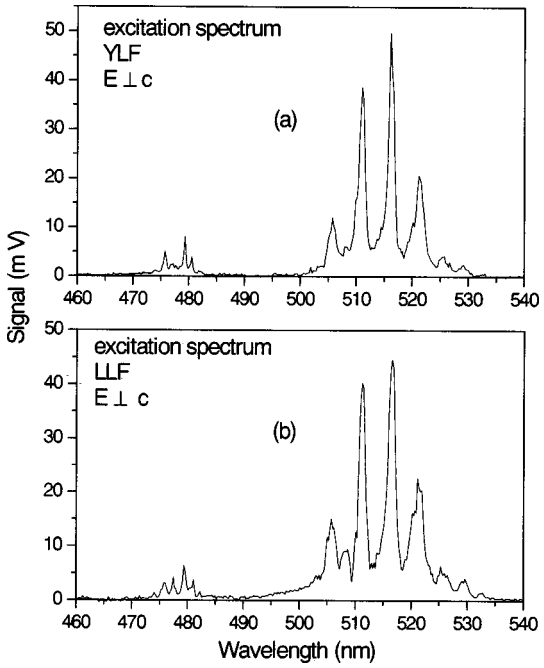

FIG. 2. Measured excitation spectra of Nd^{3+} in YLF and LLF crystals with the c axis placed perpendicular to the electric field ($E \perp c$) (or σ polarization) of the laser excitation that has a mean energy of 10 mJ and 4 ns of pulse duration and 10 Hz at 300 K.

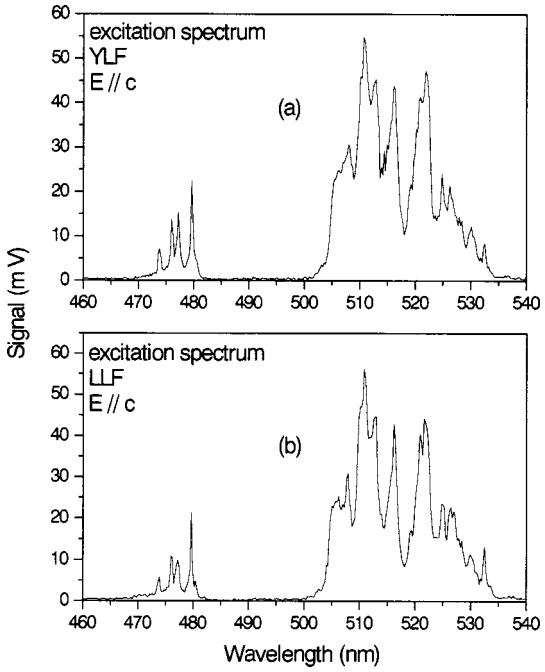

FIG. 3. Measured excitation spectra of Nd^{3+} in YLF and LLF crystals with the c axis placed parallel to the electric field ($E \| c$) (or π polarization) of the laser excitation which has a mean energy of 10 mJ and 4 ns of pulse duration and 10 Hz at 300 K.

that the laser beam does not introduce any color centers in the lattice that could contribute to the excitation spectrum measured. The excitation spectrum of 262 nm fast emission was measured using two laser excitation symmetries. In the first case, the crystal is placed with the c axis parallel to the electric field of the laser radiation ($E \| c$) or π polarization, and in the second case, the crystal was positioned with the c axis perpendicular to the laser ($E \perp c$) or σ polarization. The electric field of the laser is always horizontal. Significant differences were observed in the measured polarized excitation spectra. Figure 2 shows the excitation spectrum measured in the σ polarization for YLF and LLF at 300 K. It is observed that there are two excitation bands (green and blue) composed of well-separated narrow lines. The excitation spectrum measured in the π polarization is showed in Fig. 3. In this case, the two bands exhibited fewer structures indicating much less restriction in the excitation wavelength to reach the first and second states of $4f^2 5d$ configuration of Nd^{3+} than certainly occur in the σ polarization excitation. In addition, we observed that the σ-polarized excitation band of Nd^{3+} in the green extends up to 490 nm for LLF, while this band extends to 500 nm in YLF [see Figs. 2(a) and 2(b)]. The longest tail observed in the green excitation band of Nd^{3+} in LLF, in comparison with YLF, indicates the participation of a phonon-assisted excitation process, involving phonon emission by the intermediated excited states of $4f^3$ configuration. Because the ionic radius of Nd^{3+} is larger than the one of Lu^{3+}, a stronger coupling with the lattice of LLF crystal is expected for Nd^{3+} in $4f^2 5d$ configuration. Consequently, the intensity of the crystalline field felt by Nd^{3+} is stronger in LLF than in YLF and the optical transitions involved should include vibronic contributions, which explains the long tail observed in the excitation spectrum in the green. Figures 4 and 5 show the excitation spectrum of the first and the second excited states of $4f^2 5d$ configuration for Nd^{3+} in YLF and LLF crystals measured at 8.5 K for comparison. Excitation measurement at 8.4 K assures that only the lowest sublevel of $^4I_{9/2}$ multiplet is populated. The second sublevel of $^4I_{9/2}$ at 132 cm^{-1} above the ground state has a population fraction of $\sim 10^{-5}$ at this low temperature. This allowed us to determine the energy position of the first and second excitation bands of $4f^2 5d$ configuration simply by multiplying the excitation energy peaks measured in the visible range by a factor of 3. The observed energy level positions of the first and second excited states of $4f^2 5d$ configuration excited by three photons process are listed in Tables I and II.

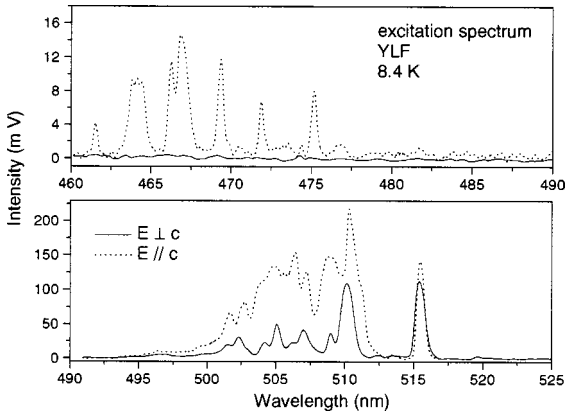

FIG. 4. Measured excitation spectra of Nd^{3+} in YLF crystals for the symmetries with $E \perp c$ and $E \| c$ under laser excitation of a pulse energy of 12 mJ and 4 ns (10 Hz) at 8.4 K.

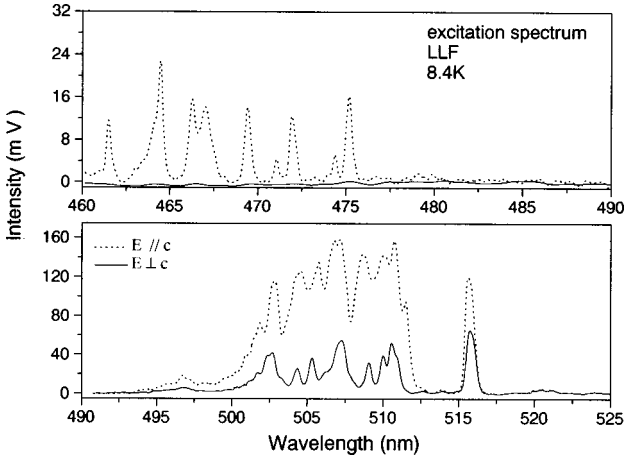

FIG. 5. Measured excitation spectra of Nd^{3+} in LLF crystals for the symmetries with $E\perp c$ and $E\|c$ under laser excitation of a pulse energy of 12 mJ and 4 ns (10 Hz) at 8.4 K.

B. Investigation of visible luminescence from the lowest excited state of $4f^25d$ configuration

Using the laser excitation in the blue tuned in 479.3 nm and pulse energy of 12 mJ, we could observe a greenish and yellowish luminescence of Nd^{3+} in YLF at 300 K. By investigating these luminescence signals using a time resolved spectroscopy we found that three excited states of Nd^{3+} contribute to the luminescence signal: $^4G_{7/2}$, $^2F(2)_{5/2}$ and the first excited state of $4f^25d$ configuration. We saw three emission bands from $^4G_{7/2}$ with peaks at 529, 590, and 620 nm exhibiting a lifetime of 8.5 ns (τ_1). The $^2F(2)_{5/2}$ excited state has an emission band with peak at 540 nm with a lifetime of 8 μs and the first excited state of $4f^25d$ configuration shows two distinct emission bands with peaks at 535 and 595 nm with a lifetime of 35 ns (τ_2). Figure 6 exhibits the luminescence decay of 590 nm emission in nanosecond scale showing the fitting by two exponential decay with constants τ_1 (9 ns) and τ_2 (34 ns). We found that 77% of the visible luminescence signal is due to the $^4G_{7/2}$ state luminescence excited by one photon process while the excited $4f^25d$(first) configuration contributes with 22% of this luminescence (three photon process). The $^2F(2)_{5/2}$ excited state excited by two photons contributes only 1% of this luminescence signal. The visible luminescence spectrum (green and yellow region) could be spectrally separated using the time resolved spectroscopy with a boxcar averager operating in static gate mode with a previous selected sample point to match the time constant of the luminescence level in observation. A sample point of 8 ns was used to discriminate the luminescence spectrum of the $^4G_{7/2}$ level and a sample point of 40 ns was used to observe the luminescence of $4f^25d$(first) configuration. The luminescence spectrum of the $^2F(2)_{5/2}$ excited state was observed using a sample point of 8 μs. Figures 7(a), 7(b), and 7(c) show the luminescence

TABLE I. Energy levels of the $4f^25d$(first) excitation band reached by three-photon excitation in Nd:YLF and Nd:LLF crystals at 8.4 K ($E\perp c$).

YLF($E\perp c$) ($T=8.4$ K) Energy level position (cm^{-1})	LLF($E\perp c$) ($T=8.4$ K) Energy level position (cm^{-1})
$4f^25d$(first)	$4f^25d$(first)
λ max(exc) = 516.2 nm	λ max(exc) = 516.3 nm
60 403.3	60 413.2
59 846.8	59 801.4
59 720.5	59 480.1
59 488.2	59 375.4
59 388.3	59 158.8
59 274.5	58 825.8
—	58 573.2
—	58 369.2

TABLE II. Energy levels of the $4f^25d$(second) excitation band reached by three-photon excitation in Nd:YLF and Nd:LLF crystals at 8.4 K ($E\|c$).

YLF($E\|c$) ($T=8.4$ K) Energy level position (cm^{-1})	LLF($E\|c$) ($T=8.4$ K) Energy level position (cm^{-1})
$4f^25d$(second)	$4f^25d$(second)
λ max(exc) = 466.5 nm	λ max(exc) = 464 nm
65 005.4	64 984.3
64 646.8	64 575.8
64 340.4	64 322.5
64 256.3	64 213.7
63 916.8	63 889.6
63 760.6	63 675.3
63 570.1	63 548.5
63 353.9	63 228.4
63 241.8	63 119.9
63 132.6	—
62 926.1	—
$4f^25d$(first)	$4f^25d$(first)
λ max(exc) = 516.2 nm	λ max(exc) = 516.3 nm
60 392.6	60 409.6
59 796.7	59 785.9
59 659.9	59 668.2
59 524.9	59 453.0
59 401.2	59 316.7
59 316.7	59 200.8
59 211.3	59 142.4
59 122.6	58 988.9
58 928.7	—
58 768.2	—
58 406.7	—
58 176.7	—

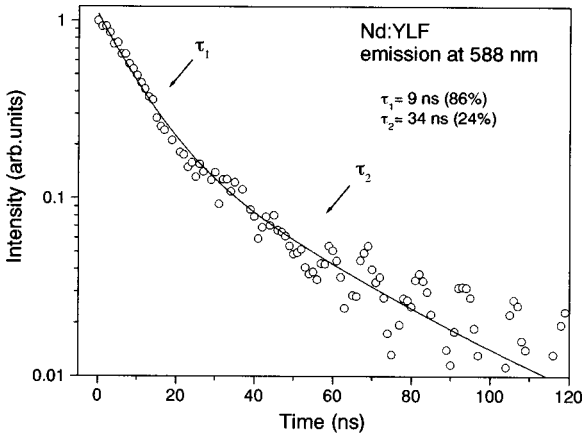

FIG. 6. Decay time of 588 nm luminescence observed in Nd:YLF crystal (at 300 K) under laser excitation with a average energy of 12 mJ exhibiting two decay components τ_1 and τ_2 related to the $^4G_{7/2}$ and $4f^25d$(first) luminescent states, respectively.

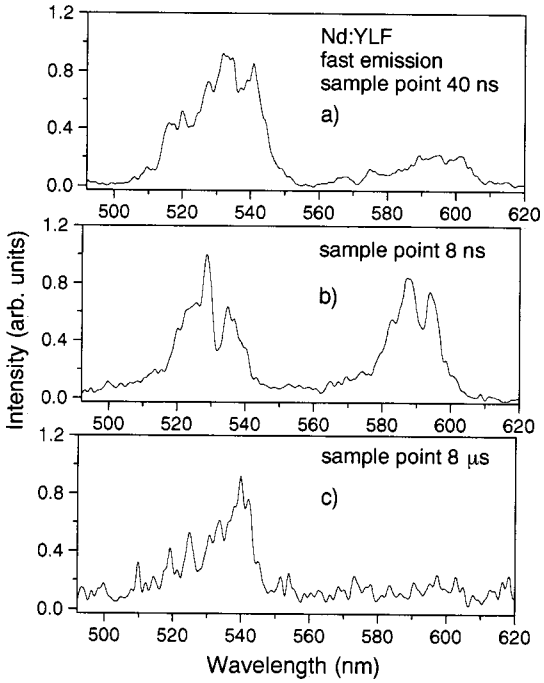

FIG. 7. Measured emission spectra in the visible range spectrally separated by using the time resolved technique. (a) Fast emission measured with a sample point (sp) of 40 ns attributed to the $4f^2 5d$(first) state decay (τ=35 ns). (b) Spectrum measured with sp=8 ns due to $^4G_{7/2}$ weak emission. (c) Slow emission component expected (τ=8 μs) for the $^2F(2)_{5/2}$ state.

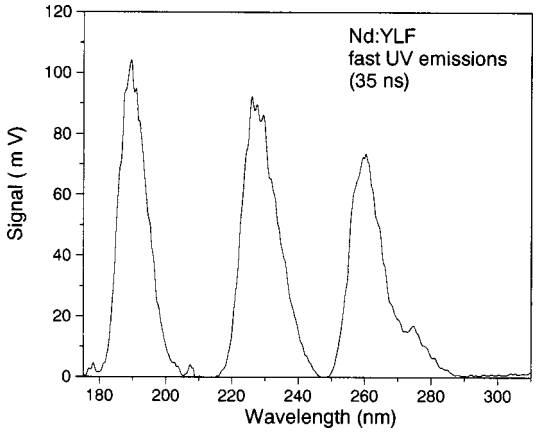

FIG. 8. The UV emission bands at 186, 230, and 262 nm of excited Nd^{3+} ions by 480 nm laser pulse of 10 mJ (10 Hz) in YLF. The exhibited spectrum was corrected taking into account the optical grating, photomultiplier (S-20 cathode) efficiencies, and the air transmittance near below 190 nm (see Ref. 25).

spectrum of the $4f^2 5d$(first), $^4G_{7/2}$, and $^2F(2)_{5/2}$ states, respectively, measured by the time-resolved luminescence spectroscopy. The laser excitation at 479 nm efficiently induces the three-photon absorption process producing the two visible emission bands at 535 and 595 nm besides the well known (180–280 nm) UV emissions. These luminescence come from the bottom of the $4f^2 5d$ configuration, i.e., the RES situated around 55 500 cm^{-1} according to the measured excitation spectrum showed in Fig. 3(b). The fast visible emissions at 535 and 595 nm have a similar lifetime of ~36 ns which is consistent with the measured lifetime of the 186, 230, and 262 nm emissions from the $4f^2 5d$ (RES). In addition, they exhibit weak polarization effects similar to the polarization effects observed for the other UV components. This weak polarization effect is expected for the $4f^n \rightarrow 4f^{n-1}5d$ allowed transitions. Both visible emissions at 535 nm (fast) and 540 nm (slow component) have a similar excitation spectrum that is also similar to the excitation spectrum measured for the fast UV emission at 262 nm. According to our observation the slow green emission at 540 nm comes from the $^2F(2)_{5/2}$ state that can be indirectly excited by the three photon process (blue laser excitation) by the fast orange emission at 595 nm. One important conclusion is that both current known luminescence branching ratios of $4f^2 5d$(RES) and $^2F(2)_{5/2}$ states must be reevaluated taking into account these emission contributions with peaks at 535, 540, and 595 nm.

C. Branching ratio of luminescence from $4f^2 5d$(RES) state

The measured spectrum of the fast UV emissions of Nd^{3+} in YLF is shown in Fig. 8. This spectrum was corrected taking into account the grating and detector efficiencies and the air transmission near 180 nm estimated for an optical path of 1.35 m, using a dry air composition ($[O_2]$ =25%) and the absorption cross section found in the literature.[25] The luminescence branching ratio was calculated by the ratio between the individual integrated band emission and the total emission area taking all the emission spectrum involved as a function of the wave number (cm^{-1}), in order to be proportional to the oscillator strength of the transition. The contribution of the emission band at 181.8 nm due to the $4f^2 5d(\text{RES}) \rightarrow {}^4I_{9/2}$ transition (not measured in this work due to the limitation of our equipment) with respect to the 186 nm emission band was taken from the literature.[21] We found that the 181.8 nm emission band is ~1.42 times more intense than the 186 nm emission band $[4f^2 5d(\text{RES}) \rightarrow {}^4I_{11/2}]$. The calculated branching ratio is shown in Table III. In this calculation we also assumed that the $4f^2 5d$(RES) state has a luminescence efficiency of 100%, because this level is situated ~7310 cm^{-1} above the nearest inferior level ($^2G(2)_{9/2}$) disabling the multiphonon decay process (N =13 if one considers the highest phonon energy of ~570 cm^{-1} observed in YLF).[26]

TABLE III. Branching ratio of luminescence from the lowest state (RES) of $4f^2 5d$ configuration in Nd:YLF (300 K), calculated taking into account all the luminescence contributions including the fast green and orange emissions reported in this article.

Fast UV emissions (nm)	β_j (exp)
182	0.24
186	0.14
230	0.20
262	0.27
535	0.11
595	0.04

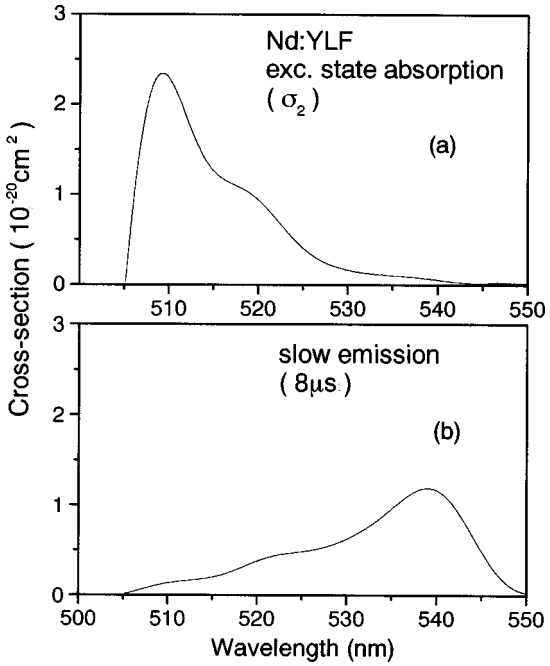

FIG. 9. The excited state absorption cross section (σ_2) due to $(^4G_{7/2};^2K_{13/2})\rightarrow{}^2F(2)_{5/2}$ transition: (a) calculated using the measured (smoothed band) emission cross section $[^2F(2)_{5/2}\rightarrow(^4G_{7/2};^2K_{13/2})]$ of Nd^{3+} in YLF (b) under laser excitation at 480 nm (10 mJ).

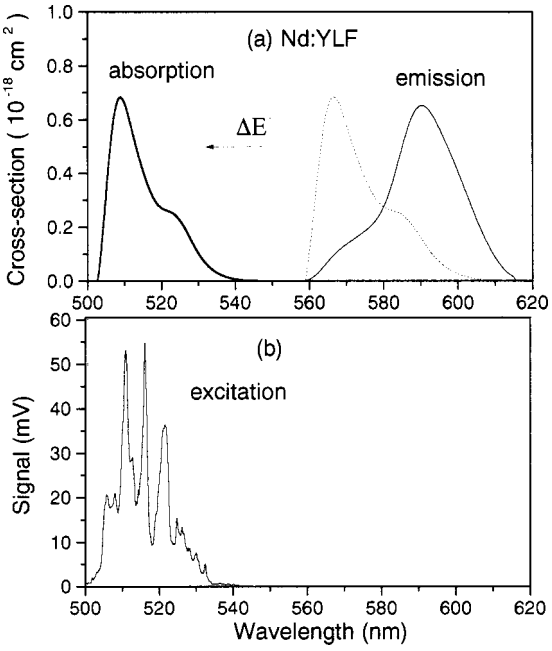

FIG. 10. The measured (smoothed band) emission cross section due to $4f^25d(\text{first})\rightarrow{}^2F(2)_{5/2}$ transition of Nd^{3+} in YLF under laser excitation at 480 nm with 10 mJ (a) (thin solid line). The reciprocal absorption cross section obtained using the McCumber relation is given by dashed line (a) and the absorption cross-section σ_3 is represented by solid curve (a) that was obtained after a blue energy shift of 2000 cm^{-1}. The measured excitation spectrum having $(\sigma+\pi)$ polarization contribution is given in (b) for comparison.

D. Determination of the multiphotonic excitation cross-section of the lowest state of the $4f^25d$ configuration

Based on the experimental observation of the upconversion UV luminescence induced by visible laser excitations we propose the following excitation sequences which leads to the bottom of the $4f^25d$ configuration:

Process 1:

$$^4I_{9/2}+h\nu'\rightarrow(^4G_{7/2},^2K_{13/2})+h\nu'\rightarrow{}^2F(2)_{5/2}+h\nu'\rightarrow4f^25d(1\text{st})$$

($h\nu'$=excitation in the green),

Process 2:

$$^4I_{9/2}+h\nu''\rightarrow{}^2G(1)_{9/2}+h\nu''\rightarrow{}^2F(2)_{7/2}+h\nu''\rightarrow4f^25d(2\text{nd})$$

($h\nu''$=excitation in the blue).

In order to estimate the equivalent excitation cross section of order three, we have to calculate the three absorption cross sections involved in this process: $\sigma_1\,(^4I_{9/2}\rightarrow{}^4G_{7/2})$, $\sigma_2\,(^4G_{7/2}\rightarrow{}^2F(2)_{5/2})$, and $\sigma_3\,(^2F(2)_{5/2}\rightarrow4f^25d(\text{first}))$. First, we should calculate the emission cross sections $\sigma_2(\text{emis})$ and $\sigma_3(\text{emis})$ using the measured spectrum $I(\lambda)$ for $^2F(2)_{5/2}\rightarrow{}^4G_{7/2}$ [Fig. 7(b)], and $4f^25d(\text{first})\rightarrow{}^2F(2)_{5/2}$ [Fig. 7(a)] transitions using Eq. (1), which relates the spectral line shape $[I(\lambda)/\int I(\lambda)]$ of the emission spectrum with the radiative transition rate $A_{ji}(s^{-1})$ by

$$\sigma_{\text{emis}}(\lambda)=\frac{\bar{\lambda}^4A_{ji}}{8\pi n^2c}\frac{I(\lambda)}{\int I(\lambda)d\lambda},\tag{1}$$

where $I(\lambda)$ is the luminescence intensity, c is the light speed in the vacuum, $\bar{\lambda}$ is the mean wavelength of the emission, and A_{ij} is the radiative transition rate, where $A_{ji}=\beta_{ji}(\tau_{\text{rad}})^{-1}$. τ_{rad} is the radiative lifetime and β_{ji} is the luminescence branching ratio of the luminescent state. The emission cross sections of 540 nm (slow) and 595 nm (fast) emission bands were calculated using the following optical parameters in Eq. (1) for YLF; refractive index $n=1.45$ for the visible range, the radiative lifetime (τ_{rad}) and the experimental branching ratio (β_{ji}) of luminescence. The values of these spectroscopic parameters used are: (i) $^2F(2)'_{5/2}\rightarrow(^4G_{7/2},^2K_{13/2})$ transition (540 nm emission): $\tau_{\text{rad}}=8\,\mu s$ and $\beta=0.25$;[27] (ii) $4f^25d(\text{first})'\rightarrow{}^2F(2)_{5/2}$ transition (595 nm emission): $\tau_{\text{rad}}=35$ ns and $\beta=0.04$ (obtained in this article). The obtained emission cross sections spectra σ_2 and σ_3 are shown in Figs. 9(b) and 10(a), respectively.

Once obtained the emission cross-section spectrum, we can calculate the equivalent absorption cross section using the reciprocity principle or the McCumber relation given by Eq. (2).[28] The principle of reciprocity which relates the absorption and emission process is valid and largely used in the case of $(4f^n-4f^n)$ optical transitions observed in trivalent rare earths ions in solids.[29–32] This is justified by the weak electron–phonon coupling of $4f^n$ configuration ($S_0<1$) so producing an emission exhibiting a small Stokes shift with respect to the absorption energy. In this case, McCumber has derived a direct relation between the absorption and emission cross sections according to the following expression:

$$\sigma_{\text{abs}}(\lambda)=\sigma_{\text{emis}}(\lambda)\frac{N_u}{N_l}\exp\left(\frac{h\nu}{kT}\right),\tag{2}$$

where (N_u/N_l) is the ratio between the upper (N_u) and lower (N_l) state populations obtained in the equilibrium temperature T; $h\nu$ is the photon energy of the transition, which is

directly related to the emission wavelength; and k is the Boltzmann constant. The equilibrium populations are obtained using

$$N_l = \sum_i g_i \exp\left(\frac{-E_i}{kT}\right), \qquad N_u = \sum_j g_j \exp\left(\frac{-E_j}{kT}\right). \tag{3}$$

Nevertheless, the procedure determined by Eq. (2) to estimate the absorption cross section for the case of $(4f^n - 4f^{n-1}5d)$ optical transition of triply ionized rare earth ions needs a small modification. One should expect an intermediate electron–phonon coupling $(1 > S_0 < 6)$ for this mixture configuration, which leads a lattice relaxation around the excited ion that happens well after the absorption process by multiphonon emission. For the case of $4f^2 5d$(first) configuration of Nd^{3+} in YLF crystal, we found a Stokes shift of $\sim 2000\ cm^{-1}$ that gives an electron–phonon coupling $S_0 \sim 3.5$, considering that the phonon emission process is mediated by the highest phonon energy ($\sim 570\ cm^{-1}$). This lattice relaxation of around the $4f^2 5d$(first) configuration produces a RES from where all the spontaneous emissions (UV and green and orange emissions) occur. Now the reciprocity principle can be applied to relate the emission and the absorption cross sections involving only the relaxed excited state $4f^2 5d$ and the final $4f^3$ state. The absorption cross section obtained in this case corresponds to the reciprocal absorption that can be calculated using Eq. (2). The real absorption cross section is evaluated by shifting the absorption wavelength towards higher absorption energy by ΔE (that represents the energy dissipation in the lattice relaxation). Equation (4) synthesizes this method. The absorption cross section obtained by this method gives a good approximation of the real absorption spectrum structure if the level structure of the upper excited level is preserved after lattice relaxation to produce the RES. Therefore, this method is valuable to calculate the absorption (cross section) spectrum of high-excited states that can be hard to measure. This method is given by

$$\sigma_{\text{abs}}(\lambda') = \sigma_{\text{abs}}^{(\text{RES})}\left(\frac{1 + \lambda \Delta E}{\lambda}\right), \tag{4}$$

where λ' is the absorption wavelength (before the lattice relaxation) and λ is the absorption involving the $4f^n \rightarrow 4f^{n-1}5d$(RES) transition (reciprocal absorption), and ΔE is the Stokes shift observed between the absorption and emission processes. The excited state absorption cross-sections σ_2 and σ_3 were calculated using Eqs. (2), (3), and (4). The populations N_l and N_u were calculated at $T = 300\ K$. The degeneracy of $4f^3$ states, given by $2J+1$, and the mean energy of the levels of the transition are: $\overline{g_l} = 10$, $\overline{E_l} = 19\,128\ cm^{-1}$ for $(^4G_{7/2}; {}^2K_{13/2})$ states, and $g_u = 6$, $E_u = 38\,640\ cm^{-1}$ for $^2F(2)_{5/2}$ used for σ_2(abs). However, the estimation of $\overline{g_u}$ for the lowest state of $4f^2 5d$ configuration needs some discussion of the literature's more recent data, in order to calculate σ_3 absorption cross section for the third step of the multiphoton process. The position of the $4f^2 5d$ energy levels of the Nd^{3+} free ion has not been determined yet from gaseous spectra, but it has been estimated on the available data for the isoelectronic Pr^{2+} ion in the $4f^2 5d$ configuration.[33,34] Using this to the Nd^{3+} free ion, a decomposition of the $4f^2 5d$ configuration gives rise to $107\,(^{2S+1}L(5d))$ levels that split into $910\,(^{2S+1}L_J)$ manifolds after considering the spin–orbit interaction.[33] The $^4K_{11/2}(5d)$ state has been indicated as the lowest state of the $4f^2 5d$ configuration of Nd^{3+}.[20,21] Recent experimental and theoretical developments have been made to describe the $f-d$ excitation spectrum of light lanthanides $(n<7)$ in three host lattices (YPO_4, CaF_2, and YLF).[5,35] In this article, the $f-d$ excitation spectrum of Ce^{3+} ion was used as a probe of the crystal-field splitting and spin–orbit parameters of $5d$ electron in new hosts than LaF_3. The $5d$ electron $(l=2)$ in the S_4 symmetry of YLF host splits into four states Γ_1, $2\Gamma_2$, Γ_3, and Γ_4 according to the group theory (using Bethe's notation). Each one of these irreducible representations gives rise to a broad excitation band in the UV and VUV range due to $4f^1 \rightarrow 5d^1$ transition of Ce^{3+} in YLF crystal. The spin representation $(D_{1/2})$ is also reduced in this local symmetry into $(\Gamma_5 + \Gamma_6)$ irreducible representation. The lowest state of $4f^0 5d^1$ configuration is obtained by the direct product between the electron representation Γ_1 and the spin representation $(\Gamma_5 + \Gamma_6)$. This lowest state is a two-dimensional representation $(\Gamma_5 + \Gamma_6)$ which has a cubic parentage with the ^2E state because the S_4 symmetry is similar to D_{2d} which is a distortion of a cubic symmetry. Pieterson *et al.*[5] observed similar $f-d$ excitation bands due to the crystal-field splitting and spin–orbit coupling for Pr^{3+}, Nd^{3+}, Sm^{3+}, and Eu^{3+} in the same host lattice. They conclude that the electronic states produced by the crystal-field interaction with the $5d$ electron dominates the structure in the $f-d$ excitation spectra, even in the more complex (rare-earth ions with more than one $4f$ electron) cases, i.e., broadband with the presence of zero phonon lines seen at low temperatures, which is characteristic of vibronic transitions. The contribution of $4f^{n-1}-5d$ Coulomb interaction could add some narrower structures but it was not experimentally seen. In the case of Nd^{3+} in YLF, they observed that the $4f^2-5d$ Coulomb interaction parameter was reduced to 74% of the one calculated for the free ion. However, the crystal field parameter of the $5d$ electron was 98% of that obtained for Ce^{3+}. This means that the $5d$ electron interacts more strongly with the crystal field of YLF lattice than with the $4f^2$ configuration. By all these arguments we conclude that most of the $f-d$ excitation bands observed in Nd:YLF are due to the $5d$ crystal-field splitting and spin–orbit interaction and that the lowest state of $4f^2 5d$ configuration is reasonable represented by the twofold state $(\Gamma_5 + \Gamma_6)$. This justifies the use of $\overline{g_u} = 2$ (and $\overline{E_u} = 56\,025\ cm^{-1}$) in the calculation of σ_3 absorption cross section [Eq. (3)] from the luminescence band of $4f^2 5d(\text{first}) \rightarrow {}^2F(2)_{5/2}$ transition.

The calculated absorption cross sections σ_2 and σ_3 are shown in Figs. 9(a) and 10(a). The ground state absorption σ_1 was obtained from the absorption measurement at 300 K with $E \perp c$ having $(\pi + \sigma)$ polarization contributions.

Once having the absorption cross sections σ_1, σ_2, and σ_3 we are able to calculate the equivalent excitation cross

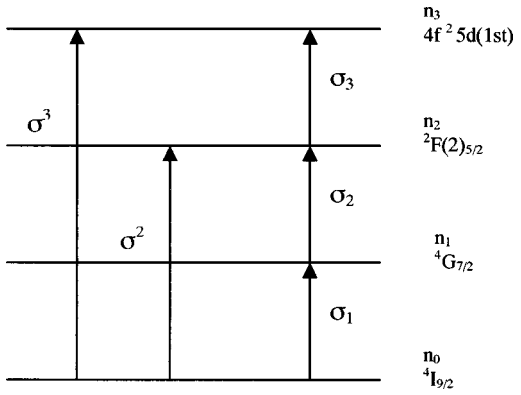

FIG. 11. A simplified energy levels diagram of Nd^{3+} in YLF is exhibited showing the four main levels involved in the three photons excitation process (at the green) and the respective multistep absorptions σ_1, σ_2, σ_3. Equivalent (or direct) excitations transitions involving two order process (σ^2) and three order process (σ^3) are also indicated by arrows. It is important to note that in this case $\sigma_3 \gg \sigma_2 \sim \sigma_1$.

section for the two (σ^2) and three (σ^3) photons process, respectively, using them in the solution of the rate equations obtained for the time scale of the laser pulse duration ($t \sim t_p$). A simplified diagram of the main levels involved in the three photon excitation is given in Fig. 11. Here the populations involved were normalized such that $n_0+n_1+n_2+n_3=1$. The following rate equations were obtained which describes the population evolution valid for $t \sim t_p$ (where t_p is the laser pulse duration and I_p is the laser intensity):

$$\frac{dn_0}{dt} = -\sigma_1 I_p n_0, \tag{5}$$

$$\frac{dn_1}{dt} = \sigma_1 I_p n_0 - \sigma_2 I_p n_1, \tag{6}$$

$$\frac{dn_2}{dt} = \sigma_2 I_p n_1 - \sigma_3 I_p n_2, \tag{7}$$

$$\frac{dn_3}{dt} = \sigma_3 I_p n_2, \tag{8}$$

where n_0 is the ground state population, and n_1, n_2, and n_3 are the populations of the excited states reached by one, two, and three absorptions of an excitation photon (green), respectively. The parameter ($I_p t_p$) is the pulse intensity of the laser excitation given in (photons/cm^2), and t_p is the laser pulse duration (4 ns). Considering the initial conditions that $n_0=1$ and $n_1=n_2=n_3=0$ for $t=0$, or $(n_0+n_1+n_2+n_3)=1$, we obtained the solutions as follows valid for the case where $t \leqslant t_p$:

$$n_0(t) = n_0 \exp(-\sigma_1 I_p t), \tag{9}$$

$$n_1(t) = \frac{\sigma_1}{\sigma_2-\sigma_1} n_0[\exp(-\sigma_1 I_p t) - \exp(-\sigma_2 I_p t)], \tag{10}$$

$$n_2(t) = \frac{\sigma_1\sigma_2}{\sigma_3(\sigma_2-\sigma_1)} n_0[\exp(-\sigma_1 I_p t) - \exp(-\sigma_2 I_p t)]. \tag{11}$$

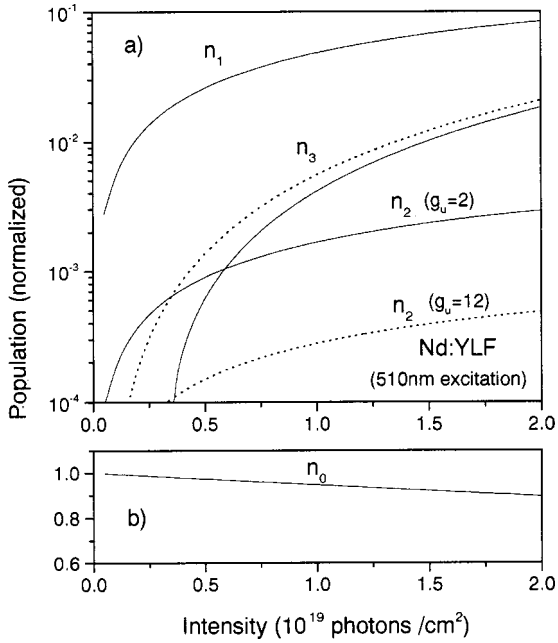

FIG. 12. The normalized populations, n_0, n_1, n_2, and n_3 are calculated by solving the rate equations of the system as a function of the laser excitation intensity at 510 nm. n_2 and n_3 are due to two- and three-photon processes. The intensity used in this work was 6×10^{18} photons/cm^2 (at 510 nm) given an excitation efficiency ($\eta=n_3$) equal to 0.10% calculated for the three-photon process.

Using the principle of population conservation obtained right after the laser excitation, we could estimate $n_3(t)$, where $n_3(t)=1-[n_0(t)+n_1(t)+n_2(t)]$, given

$$n_3(t) = 1 - \exp(-\sigma_1 I_P t) - \frac{\sigma_1(\sigma_3+\sigma_2)}{\sigma_3(\sigma_2-\sigma_1)} \exp(-\sigma_1 I_p t) + \frac{\sigma_1(\sigma_3+\sigma_2)}{\sigma_3(\sigma_2-\sigma_1)} \exp(-\sigma_2 I_p t). \tag{12}$$

The normalized populations of levels 0, 1, 2, and 3 involved in the multiphotonic excitation by two, and three photons processes, calculated as a function of the pumping intensity ($I_p t_p$ in photons/cm^2) at 510 nm; t_p is the pulse duration time, are exhibited in Figs. 12(a) and 12(b). In this calculation, the following values of absorption cross sections were used: $\sigma_1=5.54\times10^{-21}$ cm^2, $\sigma_2=2.29\times10^{-20}$ cm^2, and $\sigma_3=6.6\times10^{-19}$ cm^2. Figure 12(a) shows that the population n_3 (three-photon process) overcomes n_2 (two-photon process) for the pumping intensities ($I_p t_p$) beyond 5.9×10^{18} photons/cm^2 estimated from the solid lines crossing calculated using $g_u=2$ [the most probable description of $4f^2 5d$(first) state]. Dotted lines of Fig. 12(a) show the calculated populations using the $^4K_{11/2}(5d)$ state of free Nd^{3+} ion ($g_u=12$) if the $f-d$ Coulomb interaction could be considered stronger than the $5d$ crystal field splitting, which in fact has not been experimentally observed. Besides the two different values of g_u (2 and 12) used in this calculation, the results show that n_1 and n_3 exhibit a slight variation ($n_3=1.0\% \rightarrow 1.2\%$) while n_2 exhibits a stronger variation ($n_2=0.23\% \rightarrow 0.039\%$, respectively). The calculation (using $g_u=2$) predicts that the n_3 population equals the population of the ($^4G_{7/2}$;$^2K_{13/2}$) state (n_1) for a pumping intensity of

TABLE IV. Multiphotonic processes efficiencies and the equivalent excitation cross section obtained from the solution of the rate equation model for two- and three-photon processes for two laser excitations at 510 and 521 nm and with four pumping intensities (photons/cm^2) for Nd:YLF crystal at 300 K.

Multiphoton process (order)	Pumping intensity (photons/cm^2)	Excitation cross section (cm^2) (λ=510 nm)	Excitation cross section (cm^2) (λ=521 nm)	Process efficiency (%) (λ=510 nm)
1	0.5×10^{19}	5.54×10^{-21}	7.9×10^{-21}	2.58
	1.0×10^{19}	⋯	⋯	4.81
	1.5×10^{19}	⋯	⋯	6.73
	2.0×10^{19}	⋯	⋯	8.38
2	0.5×10^{19}	3.2×10^{-22}	7.2×10^{-22}	0.10
	1.0×10^{19}	2.9×10^{-22}	6.4×10^{-22}	0.17
	1.5×10^{19}	3.3×10^{-22}	6.9×10^{-22}	0.23
	2.0×10^{19}	2.1×10^{-22}	6.2×10^{-22}	0.29
3	0.5×10^{19}	3.4×10^{-22}	6.0×10^{-23}	0.06
	1.0×10^{19}	9.6×10^{-22}	2.8×10^{-22}	0.41
	1.5×10^{19}	1.7×10^{-21}	8.9×10^{-22}	1.00
	2.0×10^{19}	2.0×10^{-21}	1.2×10^{-21}	1.82

6.6×10^{19} photons/cm^2 (i.e., in this case $n_3=n_1=0.15$). As long as the pumping intensity increases beyond this value, n_3 tends to saturate to the unit. The efficiency of the three photon process below the damage threshold in YLF (2.2 GW/cm^2 or 2.2×10^{19} photons/cm^2) for four pumping intensities is shown in Table IV. It is important to know that the efficiency of the multiphotonic excitation process is equal to the normalized population obtained from the rate equations solution. The efficiencies of single, double, and triple photon absorptions follows the inequality relation $n_1>n_3>n_2$. Another rate equation for level 3 can be written using the equivalent excitation cross section (σ^3). The following solution was obtained:

$$\frac{dn_3}{dt}=\sigma^3 I_p n_0(t), \tag{13}$$

$$n_0(t)=n_0\exp(-\sigma_1 I_p t), \tag{14}$$

$$n_3(t)=n_0\frac{\sigma^3}{\sigma_1}[1-\exp(-\sigma_1 I_p t)]. \tag{15}$$

Substituting Eq. (15) into Eq. (12) and making $t=t_p$, we obtain $\sigma^3(\lambda)$ that is an excitation spectrum dependent on the integrated intensity of the laser pulse ($I_p t_p$)

$$\sigma^3(\lambda)=\sigma_1\left[1+\frac{\sigma_1}{(\sigma_2-\sigma_1)}\left(1+\frac{\sigma_2}{\sigma_3}\right)\frac{\exp(-\sigma_2 I_p t_p)}{1-\exp(-\sigma_1 I_p t_p)}-\frac{\sigma_1(\sigma_3+\sigma_2)}{\sigma_3(\sigma_2-\sigma_1)}\frac{\exp(-\sigma_1 I_p t_p)}{1-\exp(-\sigma_1 I_p t_p)}\right]. \tag{16}$$

Proceeding by the same way as we did to find $\sigma^3(\lambda)$, it was possible to calculate the equivalent cross section for the two photon process given

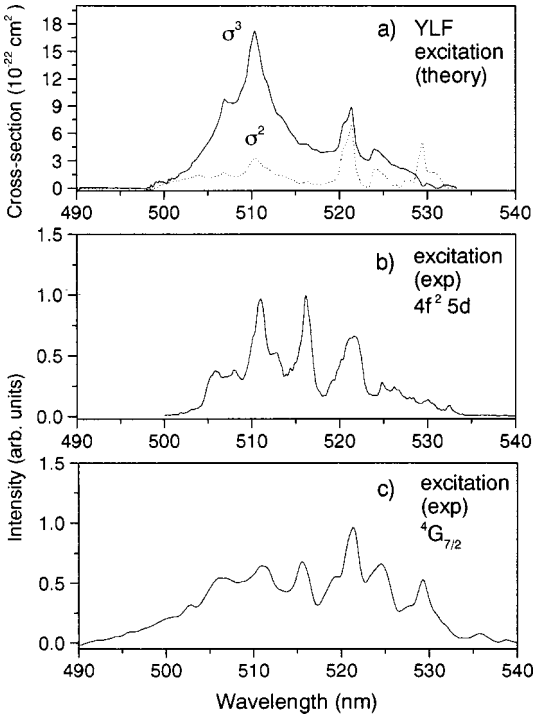

FIG. 13. (a) The equivalent excitation cross section, σ^3, obtained for the three-photon process and σ^2 for the two-photon process. They were calculated using Eqs. (16) and (17), respectively, for the laser pumping intensity of 1.5×10^{19} photons/cm^2. (b) The excitation spectrum of the three-photon process in the ($\sigma+\pi$) polarization for comparison. (c) The excitation spectrum of the one-photon process in the same polarization symmetry, i.e., the $^4I_{9/2}\rightarrow(^4G_{9/2},{}^2K_{13/2})$ transition for comparison.

$$\sigma^2(\lambda)=\frac{(\sigma_1)^2\sigma_2}{(\sigma_2-\sigma_1)\sigma_3}\left[\frac{\exp(-\sigma_1 I_p t_p)}{1-\exp(-\sigma_1 I_p t_p)}-\frac{\exp(-\sigma_2 I_p t_p)}{1-\exp(-\sigma_1 I_p t_p)}\right]. \tag{17}$$

Figure 13(a) shows the equivalent excitation cross sections (σ^3) calculated using Eq. (16) for the pumping intensity of 1.5×10^{19} photons/cm^2. One can establish a comparison between the calculated excitation spectrum $\sigma^3(\lambda)$ with the ($\pi+\sigma$) polarized excitation spectrum of $^4G_{7/2}$ state (one photon process) [see Fig. 13(c)]. We can also compare the calculated $\sigma^3(\lambda)$ spectrum with the measured three-photon excitation spectrum [($\pi+\sigma$) polarized] in the green region. The ($\pi+\sigma$) polarized excitation spectrum was composed of the sum of the σ and π polarized excitation spectra. The results exhibited in Fig. 13(a) show that the calculated spectrum of $\sigma^3(\lambda)$ is quite similar to the measured excitation spectrum of Fig. 13(b), with the exception that the calculated excitation spectrum ($\sigma+\pi$) does not exhibit a peak at 516 nm which is distinctly observed in the experimental excitation spectrum. For instance, the 516 nm peak is observed in the excitation spectrum of the $^4G_{7/2}$ state—the first absorption step of the multiphoton process exhibited in Fig. 13(c)—but does not appear in the absorption spectrum. This effect might indicate that this peak is due to a phonon-assisted optical transition which is present in laser excitation of higher intensity. In addition, a possible reduction of the fine structure of the $4f^2 5d$(first) configuration caused by the lattice relaxation to

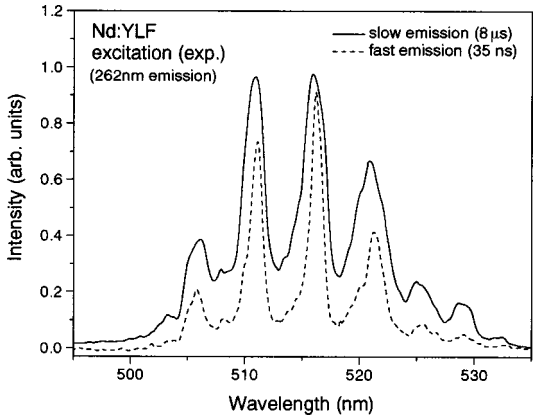

FIG. 14. π-polarized excitation spectrum of the fast (35 ns) (dashed line) and slow (8 μs) (solid line) components of the 262 nm emission for comparison. One can see that they have the same peak structure, which indicates that the three-photon process dominates the second order excitation process, as expected by the theoretic calculation that showed a level population n_3 higher than n_2 right after the laser pulse ($t \sim t_p$).

produce the RES from where the emission spectrum σ_3 was measured and consequently, σ_3(abs) was obtained, cannot account for this excitation peak missing because we have seen that the σ_3(abs) structure change can only introduce small changes in the σ^3 excitation spectrum. This is justified by the fact that $n_2 \ll n_0$ as is seen in Fig. 12(a).

E. Comparison between the excitation spectra of fast and slow luminescence at 262 nm

Figure 14 shows the excitation spectrum of the UV luminescence measured at 262 nm, decomposed in two components (fast and slow). The fast one (dashed line) comes from the $4f^2 5d$(first) configuration and the slow (solid lines) comes from the $^2F(2)_{5/2}$ level. One can see that both excitation spectra have similar spectrum profile. This suggests that the excitation spectra of the two-photon process also have contributions from the three-excitation process. As a consequence, the $^2F(2)_{5/2}$ state, which is the luminescence probe for the two-photon process, also is populated by some optical transition from the superior levels reached by the three-photon process. Looking more carefully at both π-polarized excitation spectra exhibited in Fig. 14, one verifies that the spectrum of the fast emission has deeper valleys among the excitation maximums in comparison to the spectrum of the slow component. This evidences greater wavelength selectivity in the three-photons excitation process in comparison to the two-photon process.

IV. CONCLUSIONS

The multiphoton excitation processes of Nd^{3+} in YLF and LLF crystals were investigated and a new three stepwise photon excitation in the blue spectral range was found and characterized besides the previous investigation of multiphoton excitation of Nd:YLF in the green region found in the literature.[13] The polarization effects in the excitation spectrum were investigated for both σ and π symmetries. Two emissions were discovered in the green region from $^2F(2)_{5/2}$ (slow component) and $4f^2 5d$(RES) states (fast component), which modifies the branching ratio of luminescence of the bottom of the $4f^2 5d$ configuration. The possibility of three-photon excitation in the blue spectral range made it possible to observe luminescence contributions in the region of the second harmonic of the Nd:YAG laser (532 nm). By solving the rate equations of the system under multiphotonic excitation, we were able to obtain the equivalent excitation cross section and the efficiency of the two- and three-photon processes as a function of the pumping intensity. The theoretically calculated spectrum cross section of the three-photon process to the nonpolarized excitation spectrum was measured for Nd^{3+} in YLF and LLF crystals. The pumping intensity used (0.5 GW/cm^2) produced by a pulse laser energy of 10 mJ slightly focused into the sample ($\sim$0.5 mm^2) was enough to induce the multiphoton process and allowed the luminescence measurement with a good signal to noise ratio without damaging the samples. This intensity was below the damage threshold for YLF that is $\sim$2.2 GW/cm^2. The relative excitation efficiency for the three-photon process was estimated to be approximately 1.0%, and the $\sigma^3 = 1.74 \times 10^{-21}$ cm^2 for the laser pumping intensity of 1.5×10^{19} photons/cm^2 at 510 nm. This excitation cross section value is 1.84 times smaller than the excitation cross section (σ_1) for one-photon process for this pump intensity below the damage threshold. These results show that the three-photon excitation process in the green region can be used as an alternative way of pumping Nd-doped fluoride materials to generate laser action at the ultraviolet region. This mechanism seems to be very promising to construct a neodymium UV laser based in all solid-state components.

ACKNOWLEDGMENTS

The authors are grateful for the financial support from FAPESP (Grant Nos. 1995/4166-0 and 2000/10986-0) and CNPq. One of the authors (A. F. H. L.) thanks CAPES for the fellowship.

[1] P. Rambaldi, R. Moncorgé, J. P. Wolf, C. Pedrini, and J. Y. Gesland, Opt. Commun. **146**, 163 (1998).
[2] E. Sarantopoulou, A. C. Cefalas, M. A. Dubinski, and C. A. Nicolaides, Opt. Commun. **107**, 104 (1994).
[3] E. Sarantopoulou, Z. Kollia, and A. C. Cefalas, Opt. Commun. **169**, 263 (1999).
[4] L. van Pieterson, M. F. Reid, G. W. Burdick, and A. Meijerink, Phys. Rev. B **65**, 045114 (2002).
[5] L. van Pieterson, M. F. Reid, R. T. Wegh, S. Soverna, and A. Meijerink, Phys. Rev. B **65**, 045113 (2002).
[6] M. A. Dubinskii, A. C. Cefalas, E. Sarantopoulou, S. M. Spyrou, C. A. Nicolaides, R. Yu. Abdulsabirov, S. L. Korableva, and V. V. Semashko, J. Opt. Soc. Am. B **9**, 1148 (1992).
[7] M. F. Joubert, Y. Guyot, B. Jacquier, J. P. Chaminade, and A. Garcia, J. Fluorine Chem. **107**, 235 (2001).
[8] J. C. Krupa, I. Gerard, A. Mayolet, and P. Martin, Acta Phys. Pol. A **84**, 843 (1993).
[9] A. M. Srivastava and S. J. Duclos, Chem. Phys. Lett. **275**, 453 (1997).
[10] Y. Guyot, S. Guy, and M. F. Joubert, J. Alloys Compd. **323–324**, 722 (2001).
[11] P. W. Dooley, J. Thogersen, J. D. Gill, H. K. Haugen, and R. L. Brooks, Opt. Commun. **183**, 451 (2000).
[12] Y. Guyot, A. Collombert, T. Somatri, A. Tkachuk, and M. F. Joubert, J. Alloys Compd. **341**, 178 (2002).
[13] J. Thogersen, J. D. Gill, and H. K. Haugen, Opt. Commun. **132**, 83 (1996).
[14] A. C. Cefalas, M. A. Dubinskii, E. Sarantopoulou, R. Yu. Abdulsabirov, S.

L. Korableva, A. K. Naumov, V. V. Semashko, and C. A. Nicolaides, Laser Chem. **13**, 143 (1993).
[15] M. A. Kramer and R. B. Boyd, Phys. Rev. B **23**, 986 (1981).
[16] G. E. Venikouas, G. J. Quarles, J. P. King, and R. C. Powell, Phys. Rev. B **30**, 2401 (1984).
[17] S. K. Gayen and B. Q. Xie, J. Opt. Soc. Am. B **10**, 993 (1993).
[18] F. Krupke, IEEE J. Quantum Electron. **7**, 153 (1971).
[19] L. van Pierterson, M. F. Reid, R. T. Wegh, and A. Meijerink, J. Lumin. **94–95**, 79 (2001).
[20] Y. Gyuyot, S. Guy, and M. F. Joubert, J. Alloys Compd. **323–324**, 722 (2001).
[21] Z. Kollia, E. Sarantopoulou, A. C. Cefalas, A. K. Naumov, V. V. Semashko, R. Yu. Abdulsabirov, and S. L. Korableva, Opt. Commun. **149**, 386 (1998).
[22] A. A. S. da Gama and G. F. de Sá, J. Chem. Phys. **75**, 2583 (1981).
[23] R. T. Wegh, A. Meijerink, R. J. Lamminmaki, and J. Holsa, J. Lumin. **87**, 1002 (2000).
[24] I. M. Ranieri *et al.*, J. Cryst. Growth **166**, 423 (1996).
[25] R. Goody, in *Principles of Atmospheric Physics and Chemistry*, edited by M. R. Goody (Oxford University Press, New York, 1995), Chap. 3.
[26] C. de Mello Donega, A. Meijerink, and G. Blasse, J. Phys. Chem. Solids **56**, 673 (1995).
[27] C. Li, Y. Guyot, C. Linares, R. Moncorgé, and M. F. Joubert, in *OSA Proceedings on Advanced Solid State Lasers*, edited by A. A. Pinto and T. Y. Fan (Optical Society of America, 1993), Vol. 15.
[28] D. E. McCumber, Phys. Rev. **136A**, A954 (1964).
[29] A. Brenier, L. C. Courrol, C. Pedrini, C. Madej, and G. Boulon, J. Lumin. **58**, 284 (1994).
[30] L. V. G. Tarelho, L. Gomes, and I. M. Ranieri, Phys. Rev. B **56**, 14344 (1997).
[31] F. H. Jagosich, L. Gomes, L. V. G. Tarelho, L. C. Courrol, and I. M. Ranieri, J. Appl. Phys. **91**, 624 (2002).
[32] L. D. da Vila, L. Gomes, L. V. G. Tarelho, S. J. L. Ribeiro, and Y. Messadeq, J. Appl. Phys. **93**, 3873 (2003).
[33] J. Sugar, J. Opt. Soc. Am. **53**, 831 (1963).
[34] J. Sugar and J. Reader, J. Chem. Phys. **59**, 2083 (1973).
[35] M. F. Reid, L. van Pieterson, R. T. Wegh, and A. Meijerink, Phys. Rev. B **62**, 14749 (2000).